# A Nested Hydrodynamic Model Incorporating Flooding and Drying

S. Nash and M. Hartnett

Cite as:
**Nash S** and Hartnett M (2009) A nested hydrodynamic model incorporating flooding and drying. In: Topping BHV, Costa-Neves LF and Barros RC (eds.), *Proceedings of the Twelfth International Conference on Civil, Structural and Environmental Engineering Computing*, Civil-Comp Press, Stirlingshire, UK, paper 253. doi:10.4203/ccp.91.253

## Abstract

A one-way nested version of the hydrobiological model DIVAST (Depth Integrated Velocity and Solute Transport) is introduced. The nested model allows flooding and drying of intertidal areas, a process often present in areas where nesting is required but usually excluded from nested models due to the added complexity and instabilities. An overview of the nesting procedure used in the model is presented. The model was tested in Cork Harbour where extensive flooding and drying occurs and results show that the model is capable of reproducing hydrodynamic activity to a high degree of accuracy. Substantial computational savings are also achieved. It has been found that the location of nested open boundaries can significantly affect model accuracy; the placement of nested boundaries must therefore be given careful consideration. Fine and coarse grid models were used to investigate the relationship between temporal and spatial resolution and model accuracy. The results demonstrate the applicability and benefits of nesting.

**Keywords:** one-way nested model, hydrodynamics, flooding and drying, DIVAST

## 1 Introduction

One of the most common problems in hydrobiological modelling is the location of open boundaries; they must be located such that their conditions will not adversely affect model predictions in the region of interest. This problem often leads to a situation which requires a large computational domain, of which the region of interest (ROI) comprises only a small percentage. If a finite difference model is applied, the associated orthogonal finite difference grid can become very large, particularly if a high spatial resolution is required in the area of interest. In addition, a higher spatial resolution requires a higher temporal resolution. This may result in an excessively high computational cost. One common solution to this problem is the use of a nesting method. This method allows one to increase spatial resolution in a

sub-region of the model domain without incurring the computational expense of fine resolution over the entire domain.

Nested models fall into two categories, one-way (passive) and two-way (interactive). One-way models use boundary conditions for the high resolution region that have been obtained from a low resolution calculation. This class of models is also termed *passive*; the coarse resolution flow field affects the fine resolution region by providing boundary conditions for the fine grid domain, however, there is no mechanism by which the evolution in the fine resolution region can affect the flow field in the coarse grid (and hence its own boundary conditions). Two-way or *interactive* models, in addition to providing boundary conditions for the fine grid region, allow the evolution within the fine grid to influence the evolution on the coarse grid. Although there are advantages to the interactive system they are necessarily more complicated and computationally expensive [1]. A one-way model approach was therefore deemed best for this research.

As stated, models are nested in order to increase horizontal resolution in a region of interest. However, a common problem is that the regions of interest where higher resolution is required usually contain intertidal areas which periodically flood and dry. This usually means that flooding and drying, as well as occurring inside the nested domain, will also occur along portions of their open boundaries. Flooding and drying of grid cells along open boundaries tends to give rise to instabilities in model solutions and is usually avoided; most nested models to date do not incorporate flooding and drying. This omission may be acceptable when modelling hydrodynamics (depending on the spatial resolution) as areas of flooding and drying typically exhibit low hydrodynamic activity; however, when modelling water quality areas of flooding and drying are important as both sources and sinks for water quality constituents.

The DIVAST (Depth Integrated Velocity and Solute Transport) model was chosen for nested model development as it contains a robust flooding and drying routine (see Falconer and Owens [2]). It is a two-dimensional, depth-integrated hydrobiological model which simulates hydrodynamic circulation in the form of current velocities and directions and water surface elevations, and water quality in the form of oxygen, nitrogen, phosphorus and primary production cycles. The nested version of DIVAST developed by the Authors was tested using a validated model of Cork Harbour, an estuary located on the southwest coast of Ireland. Cork Harbour was selected as it contains extensive intertidal areas where continual flooding and drying occurs; any nested domain enclosing a section of coastline will therefore experience flooding and drying both within its confines and along its open boundaries. Figure 1 shows a plan view of the extents of the Cork Harbour model. Areas of mudflats exposed on spring and neap low tides are delineated.

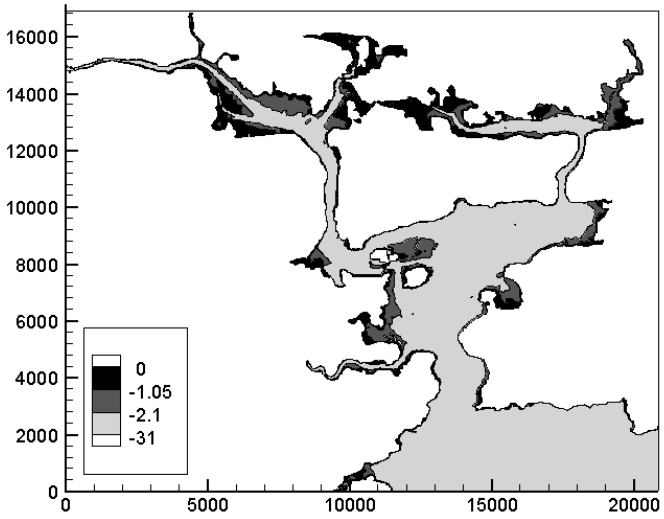


Figure 1: Cork Harbour model domain (depths in metres below mean water level) showing mudflats exposed at low neap tide (-1.05m) and low spring tide (-2.1m)

# 2 Model Details

## 2.1 Governing Equations

The governing differential equations used by the model to determine the water surface elevation and depth-integrated velocity fields in a horizontal plane are based on integrating the three-dimensional Navier-Stokes equations over the water depth. This results in a two-dimensional model which resolves variables in two mutually perpendicular horizontal directions (*x* and *y*). The depth-integrated continuity and x-direction momentum equations can be shown to be given by equations (1) and (2) respectively [3]:

$$\frac{\partial \zeta}{\partial t} + \frac{\partial q_x}{\partial x} + \frac{\partial q_y}{\partial y} = 0 \tag{1}$$

$$\frac{\partial q_x}{\partial t} + \beta\left[\frac{\partial U q_x}{\partial x} + \frac{\partial V q_y}{\partial y}\right] = \tag{2}$$

$$f q_y - gH\frac{\partial \zeta}{\partial x} + \frac{\tau_{xw}}{\rho} + \frac{\tau_{xb}}{\rho} + 2\frac{\partial}{\partial x}\left[\varepsilon H\frac{\partial U}{\partial x}\right] + \frac{\partial}{\partial y}\left[\varepsilon H\left[\frac{\partial U}{\partial y} + \frac{\partial V}{\partial x}\right]\right]$$

where, $\zeta$ = water surface elevation above mean water level
$t$ = time
$q_x$, $q_y$ = depth-integrated velocity flux components in the *x*,*y* directions
$\beta$ = momentum correction factor
$U$, $V$ = depth-integrated velocity components in the *x*,*y* directions
$f$ = Coriolis parameter

$g$ = gravitational acceleration
$H$ = total depth of water column
$\tau_{xw}$ = surface wind shear stress components in the $x$ direction
$\tau_{xb}$ = bed shear stress component in the $x$ direction
$\rho$ = fluid density
$\varepsilon$ = depth averaged turbulent eddy viscosity

The finite difference scheme used in the model is based upon the Alternating Direction Implicit (ADI) technique. This involves the sub-division of each timestep into two timesteps allowing a two-dimensional implicit scheme to be applied but considering only one dimension implicitly for each half-timestep, without the solution of a full two-dimensional matrix [3]. The solution scheme proceeds in the x-direction during the first half-timestep computing the water surface elevation, $\zeta$, and the x-direction velocity component, $U$. It then proceeds in the y-direction during the second half-timestep computing the water elevation and the y-direction velocity component, $V$. A space-staggered orthogonal grid system is used with water elevation located at the grid centre and with velocity components, $U$ and $V$, located at the centre of the grid sides. Water depth, $H$, is also specified at the centre of the grid sides.

## 2.2 Temporal and Spatial Resolution

The choice of temporal resolution, or timestep, for a model is dependant on the choice of spatial resolution and vice versa and both parameters influence the stability of the model solution and its accuracy. The governing relationship is the *Courant condition* which, for a shallow water wave, is expressed as:

$$C_n = \frac{\Delta t}{\Delta x}\sqrt{gH} \leq C \qquad (3)$$

where $C_n$ is the Courant number, $\Delta t$ is model timestep, $\Delta x$ is grid spacing, $g$ is gravitational acceleration, $H$ is water depth and $C$ is a constant.

In relation to model stability, explicit models are subject to the Courant stability criterion, $C_n<1$. This can be extremely prohibitive, forcing the use of unreasonably small timesteps which significantly increase computation costs. Implicit models on the other hand are not subject to the Courant stability criterion and can generally use large time- and space steps [4]. DIVAST is an implicit model and can therefore, strictly speaking, be run for any model timestep without becoming unstable.

In relation to model accuracy, DIVAST is subject to a Courant accuracy criterion which dictates the maximum permissible timestep $\Delta t_{max}$ for a chosen spatial resolution. It has been found that model accuracy starts to deteriorate substantially when the Courant number exceeds 8, and sometimes less [DIVAST manual]. Thus, for a chosen spatial resolution the following timestep constraint applies:

$$\Delta t \leq 8 \frac{\Delta x}{\sqrt{gH}} \quad (4)$$

where $H$ is the average water depth of the model domain measured below mean water level. Accuracy will increase somewhat as the timestep is reduced from $\Delta t_{max}$. However, as shown in Section 5.1, the amount of improvement that can be achieved is finite and for each reduction in timestep the improvement achieved decreases. Any gain in accuracy achieved in this manner must be offset against the resulting increase in computational time and a decision made as to whether the trade-off is worthwhile. The most effective method of improving model accuracy is to reduce the grid spacing but the associated increase in computational cost can be excessively high (if $\Delta x$ is reduced to $\Delta x/f$, computation time $t$ is multiplied by $f^2$). The use of a nested model allows one to achieve similarly significant improvements in accuracy whilst minimising the increase in computational time.

# 3 Cork Harbour Model

Cork Harbour is one of the largest sea inlets in Ireland, with just under 120 miles of coastline. It is essentially divided up into two main sections, the Upper Harbour, consisting of Lough Mahon, and the Lower Harbour, or Cork Harbour proper (see Figure 2). These two sections are connected by channels to the west and to the north and east of Great Island. The River Lee is the main river entering Cork Harbour. The bulk of the outflow from the upper section passes through the west channel (Passage West) and the main freshwater influence on the north and east channels, is the Owenacurra River. The Harbour is relatively deep and long, with a large surface area, and drains a large freshwater catchment; it is a macro-tidal harbour with typical spring tide ranges of 4.2m at the entrance to the Harbour. The deepest point in the Harbour, 29m below mean water level (MWL), is found in the Main Channel, while the average water depth is 8.4m below MWL. At low water, extensive areas of mud- and sand-flats are exposed throughout the Harbour.

Two different models of Cork Harbour were used to test the performance of the nested model; the first being a fine resolution model at a 30m grid spacing and the second being a coarser resolution model at a 90m grid spacing. The same domain was used in both models measuring 21km x 17km and resulting in finite difference grids of approximately 396,000 and 44,000 cells for the fine and coarse models respectively. The fine model was calibrated and validated using field measurements at the locations shown in Figure 2. Figure 3 presents validation plots for water surface elevations and current velocities at some of the locations shown in Figure 2. More complete details of the calibration/validation process are presented in Costello et al. [5].

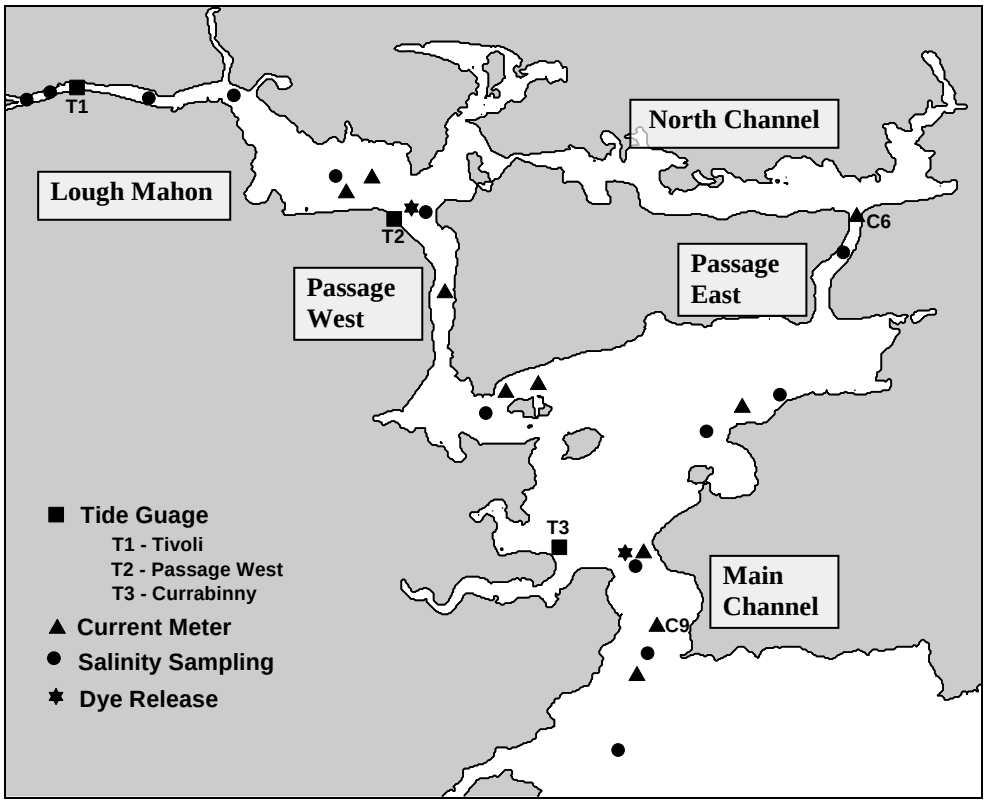


Figure 2: Plan view of model domain showing calibration/validation locations.

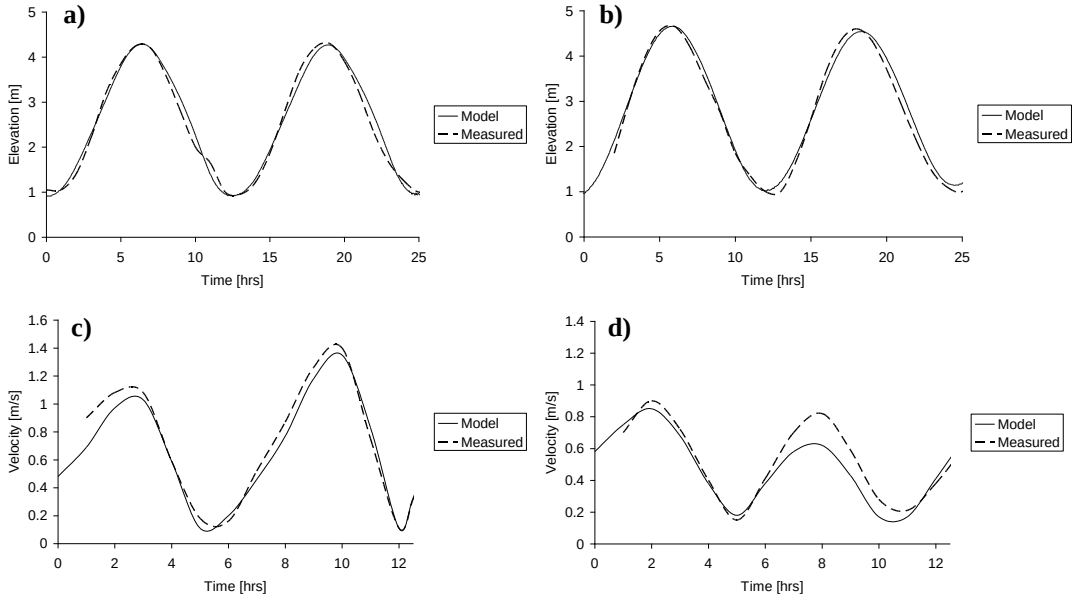


Figure 3: Validation plots: a) tidal elevation at Passage West, b) tidal elevation at Currabinny, c) current velocity at C6, d) current velocity at C9.

# 4 Nested Model

The nested model allows finer spatial resolution to be focused over a region of interest by introducing an additional grid (or grids) into the simulation. A simulation therefore involves one outer grid which contains one or more inner nested grids. Each nested region is entirely contained within a single coarser grid, referred to as the *parent* grid. The finer, nested grids are referred to as *child* grids. The model allows multiple levels of nesting, in which case children are also parents. The fine grids may be telescoped to any depth (i.e., a parent grid may contain one or more child grids, each of which in turn may successively contain one or more child grids) and several fine grids may share the same parent at the same level of nesting. Figure 4 shows an example of the grid structure for a multiply nested model. The open boundary conditions for each child grid are obtained from its parent. The nested grids allow any integer spatial ($\Delta x_{coarse}/\Delta x_{fine}$) and temporal refinements of the parent grid (the spatial and temporal refinements are usually, but not necessarily the same). The nested model is effectively a number of models running concurrently where each model operates on the set of grids at a particular level of nesting.

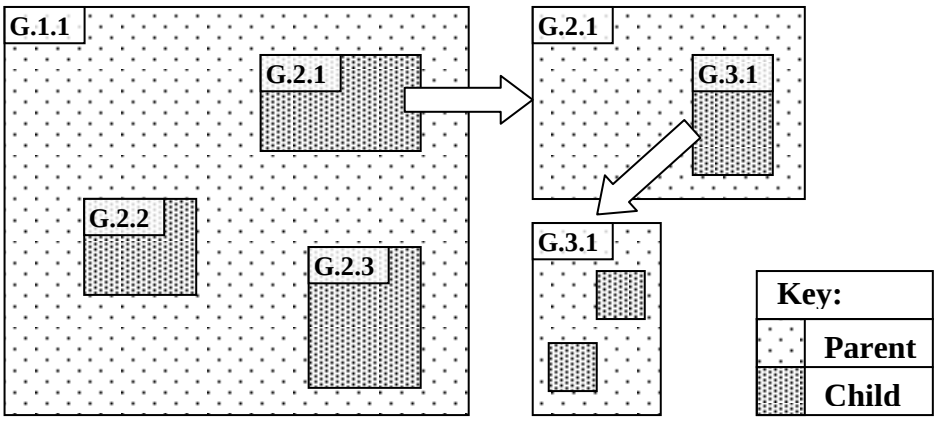


Figure 4: Nested model grid structure for multiple nesting.

## 4.1 Model Grids

DIVAST uses a space-staggered grid system as shown in Figure 5. Water surface elevation is discretised at the centre of each grid cell while water depth and normal velocity and flux components are specified at the centre of each cell interface. The implementation of the nesting procedure in the model allows the specification of any integer grid ratio ($\Delta x_{coarse}/\Delta x_{fine}$). However, an odd grid ratio is preferable as it ensures that each grid value of the overlapping region of a parent grid coincides with a value from its child grid. A schematic of a nested grid using a 3:1 grid ratio is shown in Figure 5.

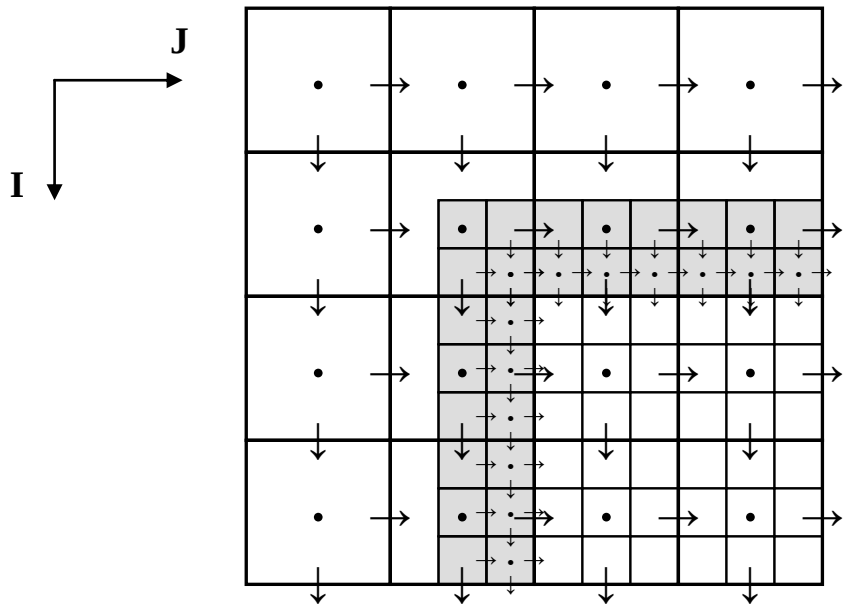


Figure 5: The relative position of the coarse (heavy lines) and fine grid (fine lines) and the halo layer (shaded). • indicates the position of elevations, → the J-direction velocity and flux components and depths and ↓ the I-direction velocity and flux components and depths. The large symbols are associated to the coarse grid and the small symbols to the fine grid. For clarity, only the positions of the variables imposed by boundary conditions are shown for the fine grid.

The interface between a parent and child grid consists of a halo layer, two fine grid cells in width; this constitutes the nested grid boundary. The nested open boundaries are driven by water elevations and current velocities obtained from interpolation of parent grid data. For the inner cells of the halo layer, elevations and velocities (both normal and tangential to the boundary) are required. For the outer cells, tangential velocities alone are required (see Figure 5).

## 4.2 Nesting Procedure

Although the model allows multiple levels of nesting, the nesting procedure is explained for clarity in the case of a single nesting. For multiple nesting, the procedure described holds for every pair of parent and child grids. The procedure is presented in graphical form in Figure 6; it can be summarised as follows:

1. integrate parent grid one timestep ($t+\Delta t_c$)
2. interpolate (time-wise) required parent grid data to current timestep of child grid ($t$)
3. spatially interpolate child grid open boundary data from parent grid data at current timestep of child grid ($t$)
4. integrate child grid one timestep ($t+\Delta t_f$)
5. repeat Steps 2 → 4 to current timestep of parent grid ($t+\Delta t_c$)

6. return to Step 1 and continue

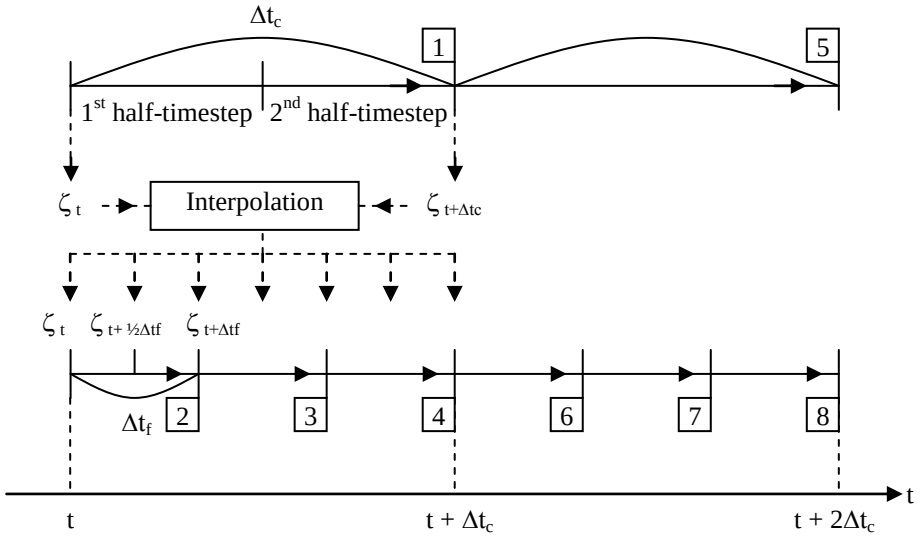


Figure 6: The nesting procedure. The subscripts *c* and *f* signify coarse and fine grids. For clarity, the only variable shown is water surface elevation, $\zeta$.

The order of time integration within the model can be seen in Figure 6. Time integration proceeds from the outermost parent grid to the innermost child. The integration of a certain parent grid can only proceed when all child grids have been integrated up to the time-level of that grid. It should be noted that DIVAST uses the Alternating Direction Implicit (ADI) solution technique to solve the governing finite difference equations; this requires that each timestep is split into two. This does not affect the order of time integration as each parent grid is integrated by one full timestep before the model proceeds to the child. However, it does affect the temporal interpolation process as each chid grid requires boundary data at each half-timestep. In relation to the interpolation of nested open boundary data, a linear technique is used for temporal interpolation while an inverse distance weighted technique is used for spatial interpolation. Both techniques have been found to give accurate results.

# 5 Model Results

Three models of Cork Harbour were developed: a coarse model, a fine model and a nested model. For simplicity the nested model had only one level of nesting with a 3:1 grid ratio. The spatial and temporal resolutions were as follows:

1. Coarse Model: $\Delta x$ = 90m, $\Delta t$ = 18s
2. Fine Model: $\Delta x$ = 30m, $\Delta t$ = 6s
3. Nested Model: Parent Grid - $\Delta x$ = 90m, $\Delta t$ = 18s
   Child Grid - $\Delta x$ = 30m, $\Delta t$ = 6s

The parent grid in the nested model was a copy of the coarse grid model with the same resolutions and hydrodynamic parameters while the child grid was a copy of the fine grid model. The fine model was assumed the 'correct solution' against which the other model results were compared.

The coarse and fine models were first used to investigate the relationship between model accuracy and resolution. The findings are presented and demonstrate the applicability and benefits of nested models. The performance and accuracy of the nested model was determined in the following manner. Coarse model results were first compared with fine model results to determine the accuracy of the coarse model. Nested model results were then compared with fine model results to determine the accuracy of the nested model. Both error analyses were then compared in order to determine the level of improvement in model accuracy achieved by using the nested model instead of the coarse. A selection of these model results are presented and discussed. The effect of nested boundary placement on model accuracy was also investigated. Results from this work are also presented and discussed.

## 5.1 Model Accuracy and Model Resolution

In order to investigate the relationship between model accuracy and resolution (both temporal and spatial) the coarse model was run for a number of timesteps ranging from 80s ($\Delta t_{max}$) to 2s and the results compared to those from the fine model. For each simulation, current velocities and water surface elevations were output at every grid cell at 30 minute intervals during the course of a spring tidal cycle (12.5hrs) giving a total of 25 hydrodynamic datasets per simulation. The accuracy of the coarse model results was determined by calculating the tidally-averaged relative error, $E_{rel}$, for the computed hydrodynamic variables. $E_{rel}$ was calculated at each grid cell *(i, j)* of the domain as follows:

$$E_{rel}^{i,j} = \frac{\sum_{n=1}^{N} \left| C_n^{i,j} - F_n^{i,j} \right|}{\sum_{n=1}^{N} F_n^{i,j}} \text{x}100 \qquad (i = 1,2,3\ldots\ i_{max} \text{ and } j = 1,2,3\ldots\ j_{max}) \qquad (5)$$

where $C_n^{i,j}$ and $F_n^{i,j}$ are the hydrodynamic variables calculated by the coarse and fine models respectively at grid cell *(i, j)* at the output time of dataset *n*. *N* is the total number of output times (*N*=25). The error analysis was carried out for both current velocities and surface elevations, however, due to space limitations only results for current velocity magnitude are presented. Figure 7 shows contour plots of the relative error of coarse model velocities for timesteps of 80s, 40s, 20s and 10s.

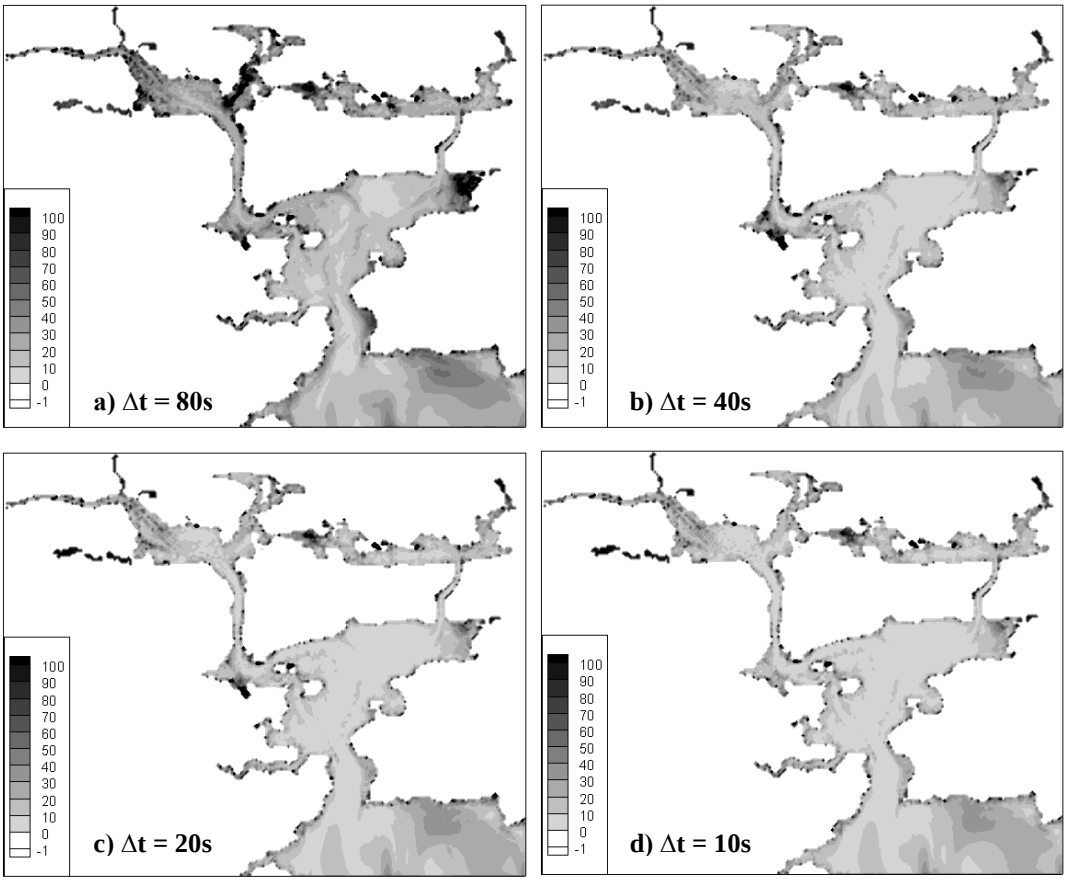


Figure 7: Relative error (%) of coarse model: current velocity magnitude.

It is particularly evident from Figures 7a and 7b that as timestep is reduced from 80s to 40s the relative error decreases domain-wide improving accuracy. This relationship is also evident when the timestep is reduced from 40s to 20s and 20s to 10s, although the reduction in error is not as significant or as visible. It can also be seen that the highest errors are found in those areas near the coastline, in bays and loughs and around headlands and islands. These areas are characterised by shallow water depths and flooding and drying. Improvements in model accuracy are slow to occur in these areas, if at all, with reduction in model timestep alone. In order to achieve significant improvements in model accuracy in these areas a finer horizontal resolution is required. These are the areas where nesting can prove beneficial. From the error data presented in Figure 7 a relationship was developed between the reduction in error in the domain as a whole and the model timestep. The relative error at each wet grid cell was summed over the model domain and then divided by the total number of wet grid cells to give the domain- and tidally-averaged relative error, $AE_{rel}$, i.e. the average relative error per grid cell per tidal cycle. This parameter is plotted against the corresponding simulation timestep in Figure 8.

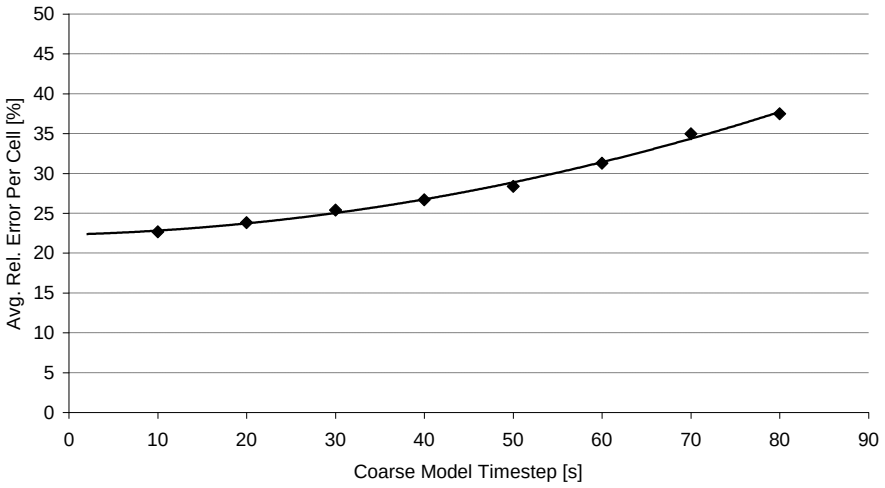


Figure 8: $AE_{rel}$ versus model timestep. (Trendline fit: $r^2 = 0.99$)

The graph shows that a significant improvement in model accuracy, approximately 30%, is achieved by halving the timestep from 80s to 40s. However, this improvement comes at the cost of doubling the computation time. A further halving of the model timestep from 40s to 20s (and further doubling of computation time) only achieves an approximate 10% increase in accuracy. For timesteps below 20s, improvement in accuracy is negligible. Any further significant improvements can only be achieved by increasing the spatial resolution. This is demonstrated in Figure 9 which compares $E_{rel}$ for velocity magnitude for the coarse and fine models using the same 20s timestep.

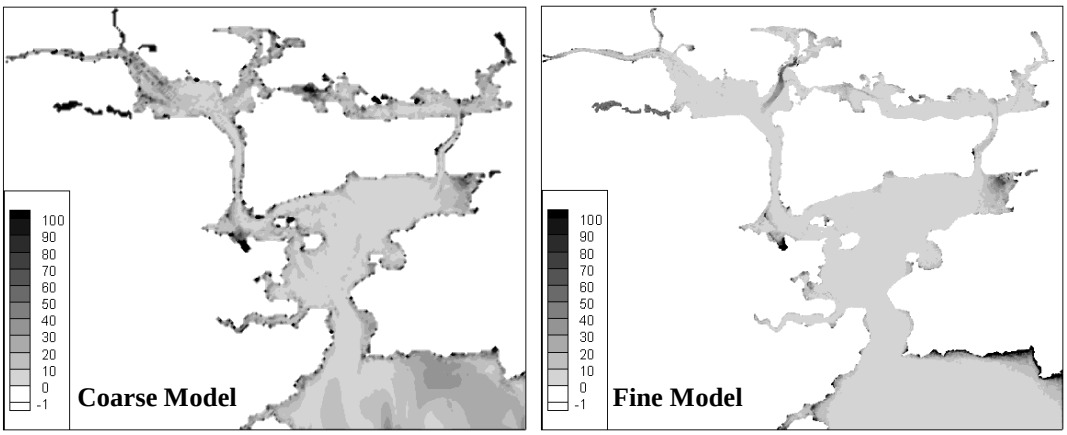


Figure 9: $E_{rel}$ (%) for velocity magnitude for coarse and fine models using $\Delta t$ = 20s.

Significant reductions in error can be observed in the diagrams. $AE_{rel}$ for the coarse model was calculated at 24%. This compares to a value of 9% for the fine model giving a 62.5% reduction in error for the reduction in grid spacing from 90m to 30m. This improvement however comes at high cost; the computation time for the fine

model is nine times that of the coarse. The use of a nested model allows one to achieve these improvements in accuracy by increasing the spatial resolution in a sub-region of the model domain without incurring the computational expense of fine resolution over the entire domain.

## 5.2 Nested Model Accuracy

Nested model performance was assessed by comparing results from the nested model with those from the coarse and fine models. In addition to testing the performance of the model in general, there was a particular focus on testing the model's performance in intertidal areas subjected to flooding and drying. Figure 10 shows the chosen nested domains, Lough Mahon and the Owenboy estuary. These areas were selected as the presence of extensive intertidal areas within their confines and along their open boundaries presented a rigorous test. The nested model was run with one parent grid ($\Delta x$ = 90m, $\Delta t$ = 18s) and two child grids ($\Delta x$ = 30m, $\Delta t$ = 6s) at a 3:1 spatial and temporal ratio. Coarse and fine models were run at corresponding resolutions for direct comparison. All simulations were run for four tidal cycles (50hrs), ensuring steady-state, and comparisons were made using the results of the final tidal cycle (37.5 – 50 hrs).

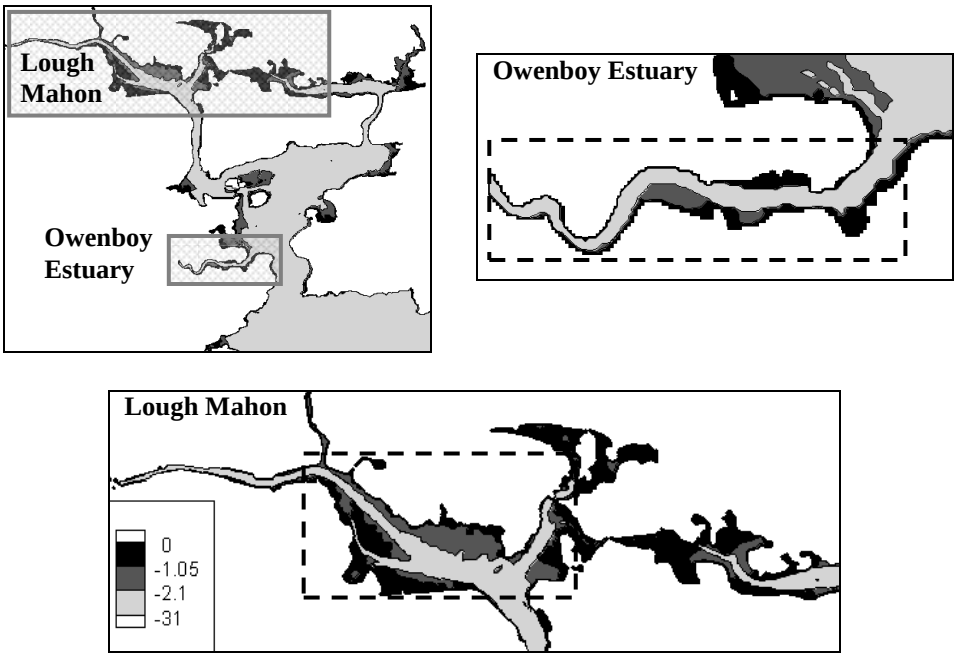


Figure 10: Extents of nested grids (shaded) and regions of interest (dashed). Mudflats on a spring tide are indicated by the -2.1m contour.

During the research, it was found that the location of open boundaries for nested domains is crucial to the accuracy of the nested model. Nested boundaries are driven by the hydrodynamic data computed by the coarser parent domain. As shown in

Figure 7, coarse domain results contain a degree of error the magnitude of which varies spatially throughout the domain. Any boundary data transferred from parent to child will therefore contain an inherent error and so any internal field calculated using this data will contain a degree of error. Through extensive model testing it was found that the boundary error does diminish with propagation into the nested domain away from the open boundary. For an accurate nested model, nested boundaries should be located sufficiently distant from the region of interest so as not to adversely affect model predictions. They should also be located in areas where the error of the coarser parent model is low. The nested boundaries in Figure 10 were selected in this way.

The accuracy of the nested model was determined by analysis of $E_{rel}$ calculated for the velocity and elevation fields computed by the nested model The level of improvement in accuracy between the coarse and nested models was also of interest and was determined by comparing $E_{rel}$ for both models. A problem when interpreting relative error data is that large relative errors are not always indicative of large inaccuracies. A small error in the prediction of a very low velocity can generate a large relative error, however, the velocity may be so low as to be insignificant in terms of overall hydrodynamic activity and the error, in absolute terms, is therefore also insignificant. To take account of this anomaly the relative error data was filtered using a second error quantity, the tidally-averaged absolute error, $E_{abs}$. $E_{abs}$ was calculated at each grid cell *(i, j)* of the nested domain as follows:

$$E_{abs}^{i,j} = \frac{\sum_{n=1}^{N} \left| C_n^{i,j} - F_n^{i,j} \right|}{N} \text{x}100 \qquad (i = 1,2,3\ldots\ i_{max} \text{ and } j = 1,2,3\ldots\ j_{max}) \qquad (6)$$

where $C_n^{i,j}$ and $F_n^{i,j}$ are the hydrodynamic variables calculated by the coarse/nested and fine models respectively at grid cell *(i, j)* at the output time of dataset *n* and *N* is the total number of output times (*N*=25). The relative error field, $E_{rel}$, was filtered by setting $E_{rel}$ to zero at those cells where the tidally-averaged absolute error was at a level deemed insignificant. This cut-off level $E_{abs}^{min}$ was taken as 3% of the average maximum velocity in the region of interest. In the case of the Owenboy estuary the average maximum velocity was 0.16m/s and $E_{abs}^{min}$ = 0.005m/s; in Lough Mahon the average maximum velocity was 0.31 and $E_{abs}^{min}$ = 0.01m/s. Figure 11 compares the filtered $E_{rel}$ for velocity magnitude for the coarse and nested models in the Owenboy Estuary. Figure 12 shows the same comparison for Lough Mahon. Relative errors were only computed within the regions of interest.

It can be seen that the relative errors of the nested velocities are significantly lower than those of the coarse model. The accuracy of the nested model is high with relative errors being less than 5% across the majority of both nested domains. Table 1 summarises the error data presented in the diagrams. In the Owenboy estuary, $E_{rel}$ for coarse model velocities was less than 5% in only 10% of the ROI compared to

99% of the ROI for the nested model; further, the nested error was less than 1% in 96% of the ROI. This suggests that the nested model is almost as accurate as the fine model. Similar levels of improvement were recorded in Lough Mahon; the coarse model error was less than 5% in only 13% of the ROI compared to 95% of the ROI for the nested model and the nested error was actually less than 1% in 92% of the ROI. The average $E_{rel}$ per cell for the nested model was only 0.2% for the Owenboy Estuary, reduced from 42% for the coarse model while that for Lough Mahon was only 0.6% for the nested model, reduced from 24% for the coarse model. All of these results suggest that the nested model performs to a high degree of accuracy.

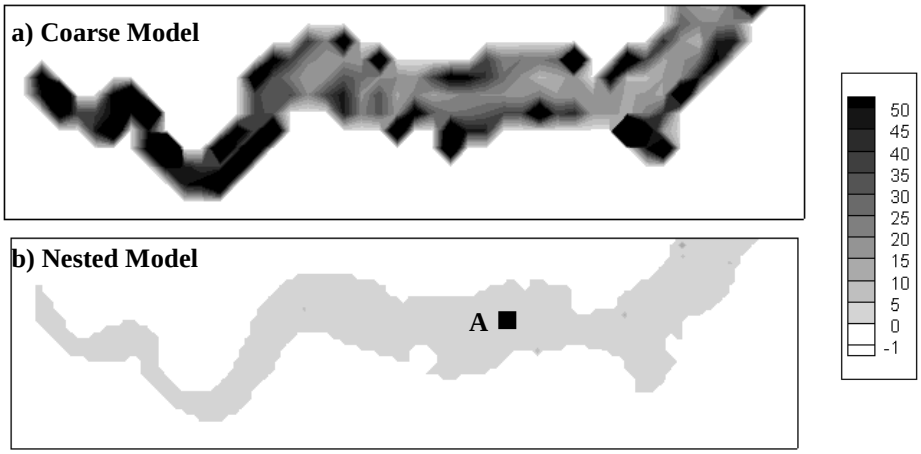


Figure 11: Filtered $E_{rel}$ (%) in velocity magnitude in Owenboy Estuary.

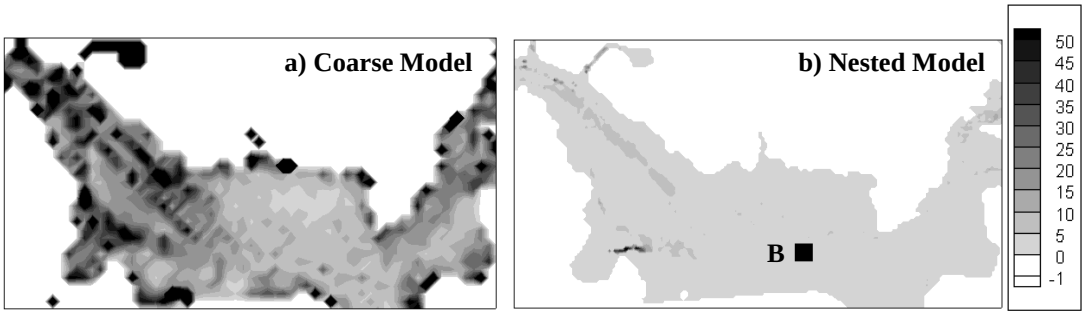


Figure 12: Filtered $E_{rel}$ (%) in velocity magnitude in Lough Mahon.

| | Owenboy Estuary | | Lough Mahon | |
|---|---|---|---|---|
| | Coarse | Nested | Coarse | Nested |
| $AE_{rel}$ [%] | 42 | 0.2 | 24 | 0.6 |
| $E_{rel}$ < 5% [% of cells] | 10 | 99 | 13 | 95 |
| $E_{rel}$ < 1% [% of cells] | 0 | 96 | 0 | 92 |

Table 1: Summary of relative error data.

As a further test of model accuracy, time series of current velocities and surface elevations were output and analysed at a number of discreet locations within the nested domains. Two of the output locations, point A in the Owenboy estuary and point B in Lough Mahon, are shown in Figures 11 and 12. Velocity and elevation data were output from the coarse, nested and fine models and the time series compared over a tidal cycle. Time series of the relative error between coarse and fine result, and nested and fine results, were subsequently calculated. The tidally-averaged relative errors ($E_{rel}$) presented earlier are an estimate of the average of these time series. Figure 13a compares velocity magnitudes computed by the three models at point A during a full tidal cycle while Figure 13b shows the error in the coarse and nested velocities relative to the fine model. Figure 14 shows similar plots for point B.

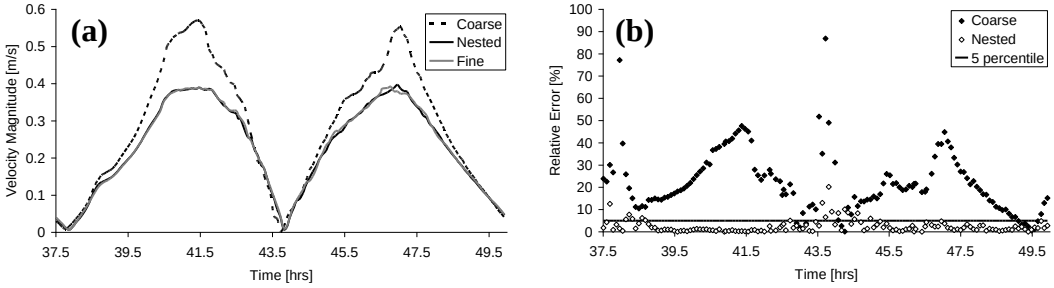


Figure 13: Comparison of velocities at point A (a) and their relative errors (b).

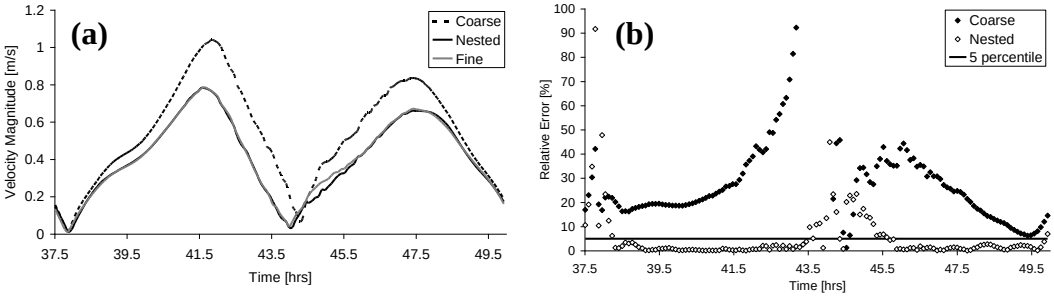


Figure 14: Comparison of velocities at point B (a) and their relative errors (b).

The time series provide further illustration of the accuracy of the nested model. While the coarse model overestimates velocities at Point A and underestimates at Point B the nested velocities are almost exact estimates of those from the fine model. It can be seen that the relative errors of the coarse model results are substantially greater than 5% for the whole of the tidal cycle while those of the nested model are less than 5% for the majority of the cycle. It should be noted that although nested errors greater than 5% are in evidence they correspond to times of slack water when velocities are almost zero and are thus insignificant. The error time series agree with the results presented in Figures 11b and 12b where it is seen that the tidal-averaged relative error of the nested velocities (i.e. the average of the time series in Figures 13b and 14b) at Point A and Point B are less than 5%.

The tidally-averaged relative errors, $E_{rel}$, were calculated using data at only 25 times. In order to confirm that they are indeed an accurate representation of the tidal average, the same parameter was calculated using the relative error time series (with 139 data points) and the values compared for each output point. The same comparison was carried out for the coarse model relative errors. Table 2 presents the values for Points A and B. It can be seen that $E_{rel}$ is an accurate estimate of the tidal-averaged relative error. A similar level of accuracy was found at all of the output locations.

| Output Points | $E_{rel}$ [%] (N=25) | $E_{rel}$ [%] (N=139) |
|---|---|---|
| Point A: | | |
| - Coarse | 31.6 | 30.1 |
| - Nested | 2.3 | 2.3 |
| Point B: | | |
| - Coarse | 24.0 | 24.1 |
| - Nested | 2.2 | 1.9 |

Table 2: Tidal-averaged relative errors in velocity magnitudes at points A and B.

It has been shown that the nested model developed by the Authors behaves well and achieves a high degree of accuracy, even in intertidal areas subject to flooding and drying. It was found, however, that model accuracy is heavily dependant on the location of open nested boundaries. To demonstrate this boundary effect, an additional simulation was run where the east and west boundaries of the Lough Mahon nested grid were moved (see Figure 15) to locations both closer to the region of interest and where the coarse model was less accurate.

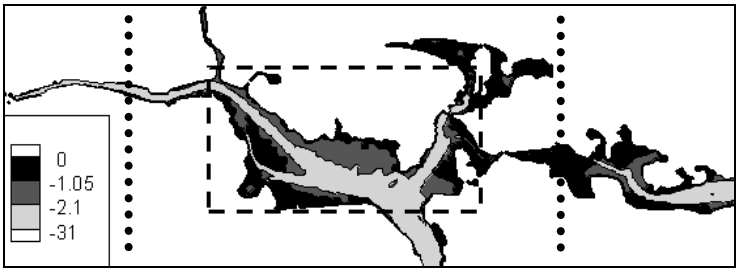


Figure 15: Lough Mahon nested grid showing new east and west boundaries.

Figure 16 compares the tidal-averaged relative error in velocities computed by the old and new nested models. The effect of the new boundaries is very apparent with a significant increase in error in certain areas of the domain; $E_{rel}$ was less than 5% in 95% of the domain for the old model compared to only 73% for the new model. The increase in error is due to the propagation of error from the new boundaries into the region of interest due to their closer proximity and the fact that the boundary data is less accurate and contains a higher level of error. The decline in

accuracy is further demonstrated by Figure 17 which compares tidal velocities from both the old and new nested models with those from the fine model at points B and C shown in Figure 16b. The magnitudes of the errors observed agree with the contoured error plots in Figure 16 which show that the model is inaccurate at both locations with a higher level of inaccuracy at point C.

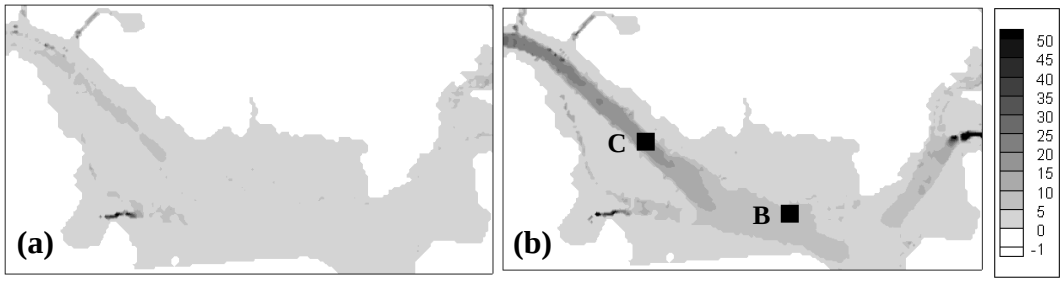


Figure 16: $E_{rel}$ (%) in velocity magnitude for the old (a) and new (b) nested models.

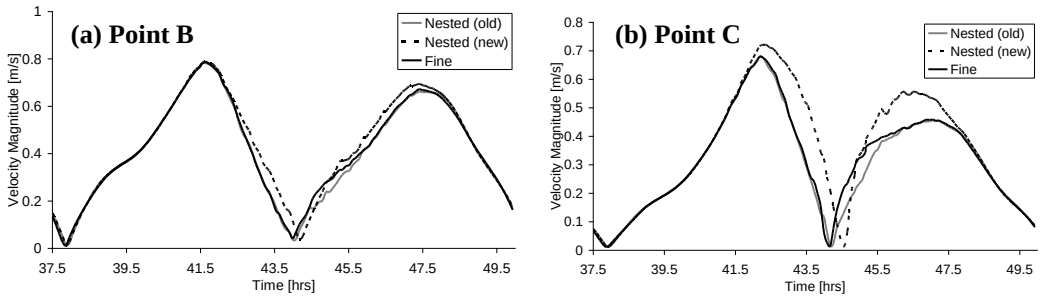


Figure 17: Comparison of velocities between nested and fine models.

# 6 Summary and Conclusions

The Author's have developed a one-way nested version of the hydrobiological model DIVAST. The nested model allows flooding and drying of intertidal areas, a process often present in areas where nesting is required but usually excluded from nested models due to the added complexity and instabilities. The model allows multiple nesting, i.e. each parent grid can have one or more child grids, each of which in turn can successively have one or more children. Extensive testing has shown that the model is stable and is capable of computing hydrodynamic activity to a high degree of accuracy. The model performed equally well in areas of flooding and drying and in deeper waters. The model also allows flooding and drying of a nested boundary; the nested boundary effectively behaves as a dynamic boundary.

The accuracy of the nested model is dependant on the location of the open boundaries of the nested domains. The nested boundaries of each child grid are driven by data obtained from its coarser parent which are inherently erroneous. These errors are passed from parent to child across the open boundary and propagate

into the child domain. The errors decrease with distance from the open boundaries and boundaries should therefore be located sufficiently distant from the area of interest so as to minimise their influence. Boundaries should also be located in areas of the parent domain where accuracy is high to minimise the error being passed from parent to child. Careful consideration should therefore be given to the location of nested boundaries. Ideally, an error analysis of the parent model, similar to that presented in Section 5.1, should be carried out to identify optimum locations for boundaries of nested grids.

Nesting is a very cost-effective method of improving model accuracy by increasing model resolution. It has been shown that for a grid spacing $\Delta x$, model accuracy can be improved by lowering the timestep $\Delta t$ which will also increase the computational effort. However, the level of improvement that can be achieved in this manner is finite and tends to zero as $\Delta t$ is lowered. Any further improvement in accuracy can only be achieved by increasing the spatial resolution, again at a high computational cost. The nested model allows one to achieve the same improvements in accuracy by increasing the resolution in a sub-region of the model domain without incurring the computational expense of fine resolution over the entire domain. The computation time for a 50hr simulation using the nested model was 78mins. This compares with a time of 278 mins for the fine model giving a computational saving of 72%. This saving becomes even more important when water quality modelling is included in the simulation. The Author's are currently developing a parallelised version of the nested model where each parent and child grid is assigned to a different processor. This will further reduce the computational cost. In addition, the Author's have developed an adaptive mesh version of the nested model (Nash and Hartnett [6]) which enables yet further reduction of the computational cost.

# References


[1] Spall, M.A. and Holland, W.R., "A Nested Primitive Equation Model for Oceanic Applications", Journal of Physical Oceanography, Vol. 21, 205-220, 1991.

[2] Falconer, R.A. and Owens, P.H., "Numerical Simulation of Flooding and Drying in a Depth Averaged Tidal Flow Model", Proceedings of Institution of Civil Engineers, Part 2, Research and Theory, Vol. 83, March 1987, pp.161-180.

[3] Falconer, R.A., Lin, B., Wu, Y. and Harris, E., "DIVAST Reference Manual", Environmental Water Management Research Centre, Cardiff University, 2001.

[4] Martin, J.L. and McCutcheon, S.C., "Hydrodynamics and Transport for Water Quality Modelling", Lewis Publishers, 1999.

[5] Costello, M.J., Hartnett, M., Mills, P., O'Mongain, E., Collier, L., Johnson, M., Nash, S., Leslie, R., Berry, A., Emblow, C., Collins, A., and McCrea, M., "Nutrient Dynamics of Two Estuaries in Ireland: Wexford and Cork Harbours", Irish Environmental Protection Agency, 2001.

[6] Nash, S. and Hartnett, M., "An Adaptive Mesh Solute Transport Model", Proceedings of the Twelfth International Conference on Civil, Structural and Environmental Engineering Computing, 2009.